The 5th European sCO2 Conference for Energy Systems
March 14-16, 2023, Prague, Czech Republic

2023-sCO2.eu-145

DESIGN AND EVALUATION OF LOW SPECIFIC SPEED EXPANDER FOR GEOTHERMAL ENERGY APPLICATION

Abhay Patil*
Southwest Research Institute, USA
Email: abhay.patil@swri.org

Jordan Nielson
Southwest Research Institute, USA

Natalie Smith
Southwest Research Institute, USA

Nathan Weiss
Sage Geosystems, USA

ABSTRACT

The increased interest in harnessing geothermal energy requires more attention to exploring and optimizing the design space for expanders with a specific focus on efficiency and reliability under off-design conditions. This study focuses on the design of a low-specific speed radial expander with a targeted shaft power of 0.5 MW at 22,000 rpm for the geothermal application utilizing CO_2 as a working fluid at 150°C. The design analysis includes exploration of the effects of loading and flow coefficients on low-specific speed expanders and iterative design optimization using coupled 3D design and CFD simulations. The 3D optimization shows that designing a turbine with higher loading enables optimal efficiency point (92% isentropic) with the desired off-design performance, however, with increased reaction thrust as the consequence of increased loading. Further CFD simulations of the entire expander control volume including front and back seals show that thrust force in the direction from outlet to inlet (upthrust) increases as the flow rates and rotational speeds reduce. The study concludes with a discussion about the control scheme for turbine start-up and the performance of low-specific speed turbines for geothermal applications.

INTRODUCTION

Significant research has been focused on investigating the use of CO_2 in power cycles for existing and future applications. Supercritical Co2 (sCO2) is dense like a liquid yet behaves like gas with compression or expansion processes occurring without phase change. Compared to steam, sCo2 is nearly twice as dense, easier to compress, and an inert and stable fluid even at very high temperatures (600°C and above). Density change due to shifts in pressure and temperature enables a large amount of energy extraction subsequently reducing equipment size with high thermodynamic efficiencies. The use of CO_2 is also beneficial to harnessing different heat sources including geothermal energy. Current methods to use geothermal energy include dry steam, flash steam, and the binary Organic Rankine Cycle (ORC) plants [1]. Dry steam and flash steam plants use steam directly to harness geothermal energy while ORC uses moderately heated geothermal fluid (~200 °C) to heat the secondary fluid. Binary power plants using ORC inherently uses a low source temperature that represents a large portion of available geothermal energy for electricity generation.

Many researchers [2][3] recently focused on evaluating the performance of ORC using different fluids and mixtures for geothermal and waste heat recovery applications. In comparison, the desirable thermophysical properties of sCO_2 for power cycles offer improved efficiencies and net power compared to the current state of the art [4]. CO_2 has desirable density, particularly near the supercritical region, at different cycle conditions as well as single phase conditions during the heat exchange process that enables the design of small-size turbomachinery and heat exchangers with a possible roadmap for optimal architecture based on source temperature [5]. Co2 Plume Geothermal (CPG) technology presents an outstanding Co2 storage option utilizing geothermal formations that exhibit desired energy potential for extraction. Part of stored Co2 is used for energy generation, and equivalent heat extraction using CPG requires less auxiliary pumping power due to an improved thermosiphon effect compared to water-based geothermal energy extraction [6], [7]. However, the reservoir permeability and temperature play a critical role in yielding competitive LCOE values compared to other established renewable energy conversion methods. The majority of geothermal sites targets mid-enthalpy (150-250°C, ~5.5 km depth) dry and sedimentary rock, accessible throughout the United States and the world. One of the envisioned thermal well architectures includes a closed-loop vertical geothermal well design with cooled fluid pumped from the surface via the outer ring for heat extraction and the inner ring for the return path for hot fluid. This ensures no hydrogen sulfide or steam leakage

* corresponding author(s)

DOI: 10.17185/duepublico/77324

during the operation and improved natural convection due to the downward fractures [8].

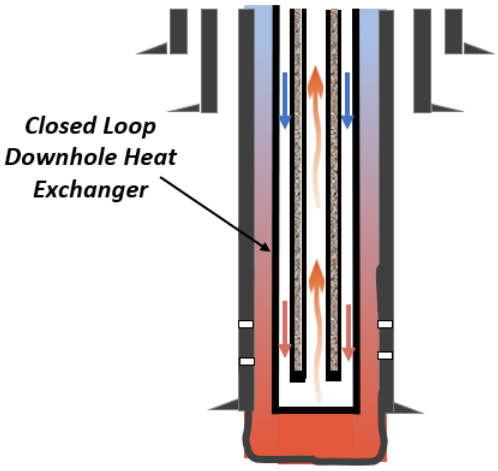

Figure 1: Closed loop geothermal well [8]

For the geothermal energy plants, the power output and turbine inlet conditions vary widely for different well conditions [9]. Additionally, fluctuations in ambient conditions and degradation in well output conditions through its life cycle will affect the turbine power output. Anticipating those factors in the design of the power generation unit and developing a modular approach that allows the operator to replace the aerodynamic portion of the turbine (without replacing the gearbox, generator, and support system) to accommodate the changing well conditions will enable optimal recovery as well as reduced time to maintenance over the well life [10]. However, using a synchronized generator requires a fixed rotational speed to meet the operational requirements. Further work focused on utilizing 1D Balje analysis to investigate the optimal rotational speed for a single-stage radial expander for different power flow conditions representing different sites. From the bounds of optimal speeds for each case, 22000 rpm was selected because it could meet the desired power output levels to achieve the required design, manufacturing, and operational flexibility (). The focus of the current study is to develop a turbine option for the lowest flow condition that will enable validation of the proposed plan under a laboratory-scale test environment. The proposed operational conditions include 15.75 MPa inlet pressure, 7.5 MPa outlet pressure, 15 kg/s mass flow rate, and 150°C inlet temperature with a fixed rotational speed of 22,000 rpm. The analysis will focus on aerodynamic design to develop an expander, nozzle, and volute for the proposed condition, 3D CFD simulations to quantify the performance, and the development of a full numerical model including balance piston seals to quantify the shift in performance as well as prediction of thrust for the proposed operating conditions.

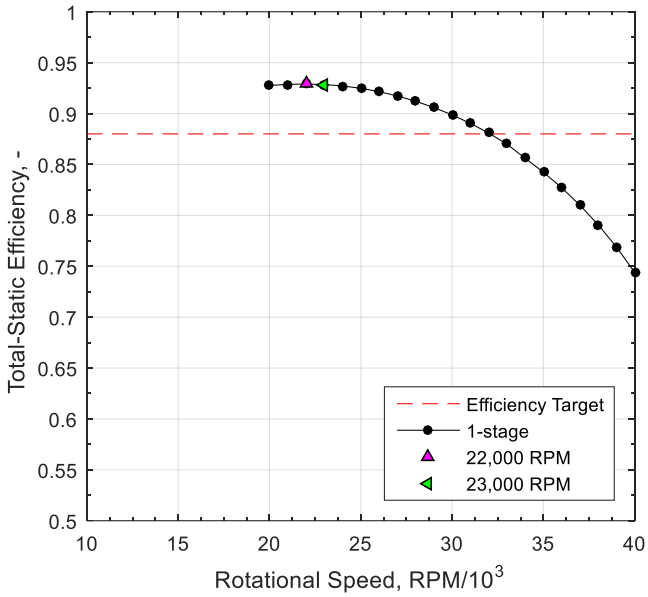

Figure 2: 1D Balje analysis of the rotational speed at lower flow case [10]

DESIGN METHODOLOGY AND THE DESIGN RESULTS

Operating conditions and constraints from cycle modeling with well conditions are used to define preliminary turbine design parameters. The 1D turbine design process initiates by using these parameters as input conditions, and the 1D modeling outcomes are fed to the 3D design optimization process from which the final detailed design is obtained after iterations. The approach is shown in Figure 3.

An in-house pseudo-1D aerodynamic design tool based on the experience chart is used to develop initial estimates for the rotor geometry. The tool uses head and flow coefficients with assumed values of total-to-total efficiencies to calculate velocity triangles at the inlet and outlet based on desired outlet pressure. The tool doesn't account for any loss mechanisms, but rather uses a combination of loading and flow coefficients to output the geometry parameters within the given bound of geometrical and velocity constraints at the inlet and outlet for an initial estimate of the optimal design.

The design procedure is outlined in Baines, 2005 [11]. Figure 4 shows the total-to-static efficiency correlation with these coefficients and how this design compares with experience. The experience chart is a good starting point in the sense that the outcomes from testing different turbine rotors enable drawing constant efficiency lines and hence setting up a baseline for the initial design point. As for the current operational conditions, design point falls on the low specific speed side (Ns: 0.25) which requires the design selection with a larger inlet tip-to-exit tip ratio. However, the low flow conditions make it easier to achieve the optimal trade-off between friction and separation losses due to low flow instability and flow alignment from inlet to outlet. This trade-off is balanced with the iterative selection of loading and flow coefficients.

DOI: 10.17185/duepublico/77324

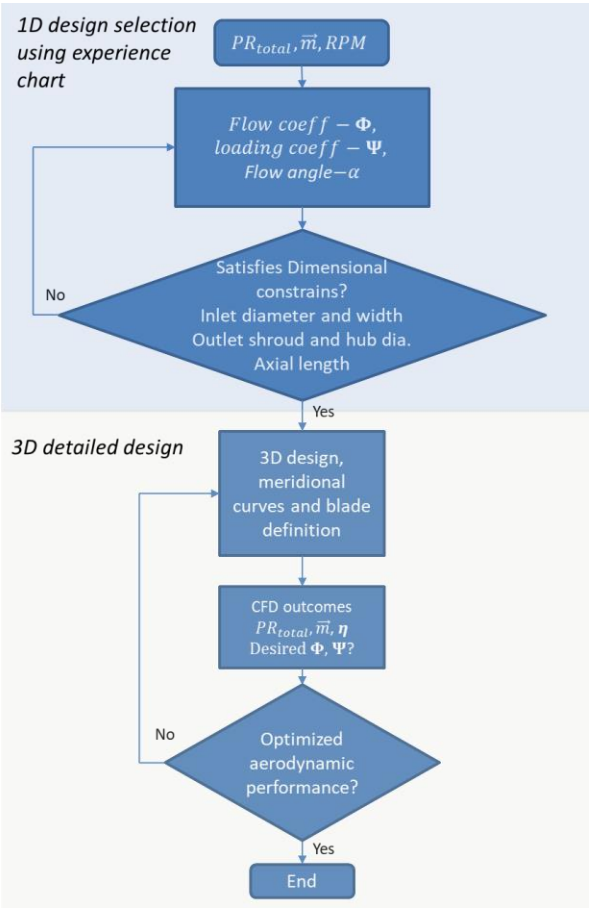

Figure 3: Expander design approach

The next step involves creating a 3D detailed design of the rotor including blade definition, nozzle, and volute. This requires an iterative approach of generating rotor geometry including blade designs and flow passages and then evaluating the different candidates using 3D steady CFD. Turbine 3D aerodynamic design definition includes hub, shroud, and blade angle profiles from inlet to outlet. CFTurbo was utilized to develop and iterate 3D aerodynamic design. The next step included developing a periodic numerical model using Turbogrid and simulation in CFX2020 R1. A mesh sensitivity study revealed a 0.5% difference between the coarse and fine mesh. Design iterations employed coarse mesh for the design optimization. The efficiency from the previous iteration is fed back to the 1D design tool to iterate the next design. Figure 6 shows the final shrouded rotor geometry and the geometric parameters. The same iterative process is employed to design the volute and nozzle to ensure the desired interaction at the stator rotor interface defined using the flow angle and slip. After the design of the rotor and volute is complete, a final transient CFD simulation is performed using Fluent 2020R1 to ensure the expected performance in terms of shaft power and efficiency at design and off-design conditions.

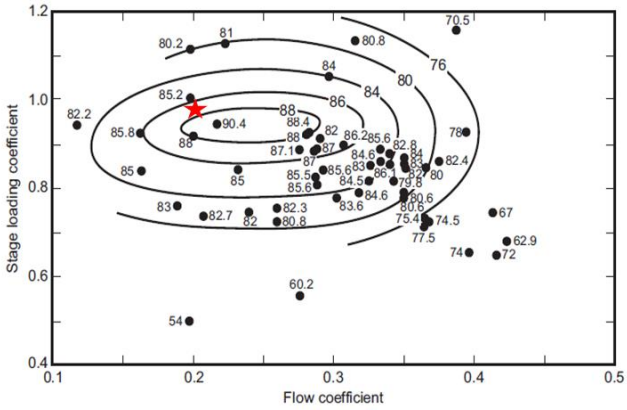

Figure 4: Correlations of blade loading and flow coefficients for radial inflow turbines (Total-to-static efficiency) [11]

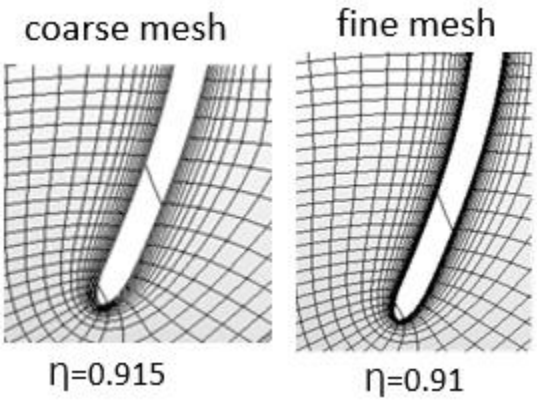

Figure 5: Mesh sensitivity

DOI: 10.17185/duepublico/77324

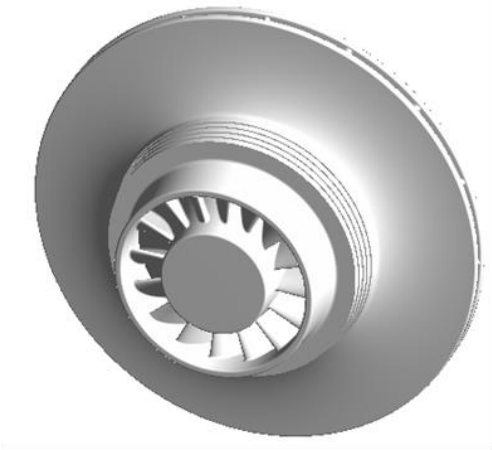

Geometric parameters	Values
Inlet diameter (m)	0.172
Outlet shroud Diameter (m)	0.072
Outlet hub diameter (m)	0.042
Number of blades	16
Average blade thickness (m)	0.00325
Axial Length (m)	0.051
Inlet Width (m)	0.0035

Figure 6: Rotor geometric information

Figure 7 shows the mesh model of the aerodynamic flow path including the volute, nozzle, and rotor. The numerical scheme employs a hybrid approach utilizing a combination of hexahedral and tetrahedral elements. Boundary conditions include total pressure at the inlet and pressure outlet. The model employs the steady-state moving reference frame to simulate the rotor rotation. The rotor zone is rotational with an assigned speed of 22,000 rpm. All other zones are stationary. K-ω SST turbulence model is employed. The pressure-velocity coupling is achieved using the SIMPLE scheme, a segregated solution method provided by Fluent. Convergence of the mass flow rate and outlet pressure are monitored to ensure the resulting residue is less than 10^-5. Figure 8 shows the meridional velocity profile at design conditions, and Figure 9 shows blade-to-blade pressure and velocity profiles at 0.5 span. Figure 10 shows the entropy generation as a result of the fluid-structure interaction. Increased entropy represents the losses and contributes to the rotor performance degradation. Increased flow velocity on the suction side surface triggers the entropy generation that extends to the rotor zone. The increased surface area due to the curved design may have been the contributing factor that may need attention in further optimization of the nozzle. In the rotor passage, slight flow separation on the suction side of the blade further triggers and extends the entropy generation into the flow field. The blade loading profile on the suction side in Figure 11 shows this effect with a slight flattening of the suction side curve on the back half of the blade. Figure 10 shows the off-design performance with the 22,000 rpm Speedline including efficiencies and shaft power at design. The design point seats on the right side of the performance curve to enable the desired efficiency outcomes over the wide range of flow conditions.

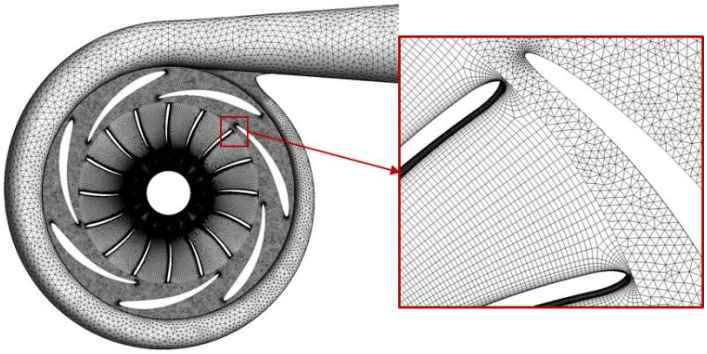

Figure 7: Mesh model

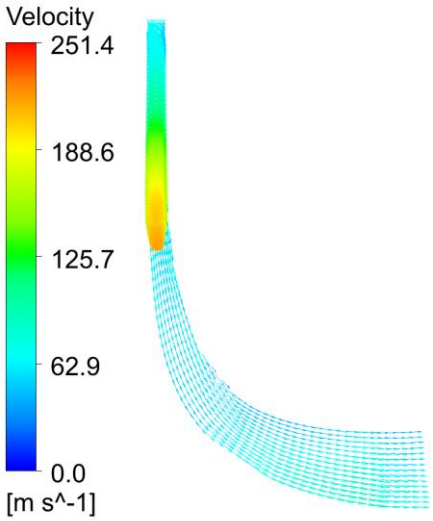

Figure 8: Meridional velocity profile

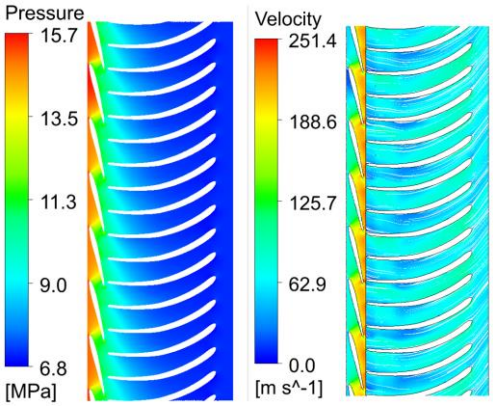

Figure 9: Blade to blade pressure and velocity profiles at 0.5 span

DOI: 10.17185/duepublico/77324

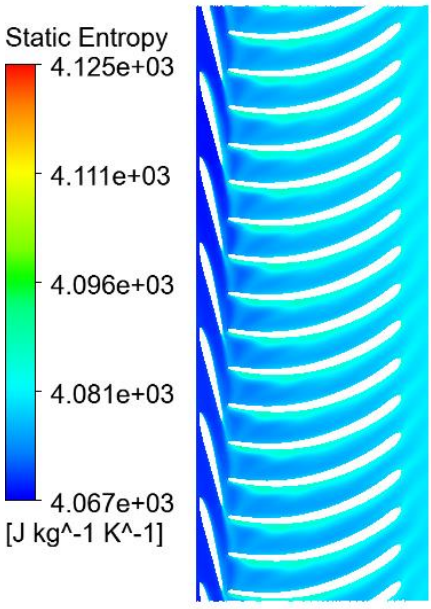

Figure 10: Entropy generation at 0.5 span

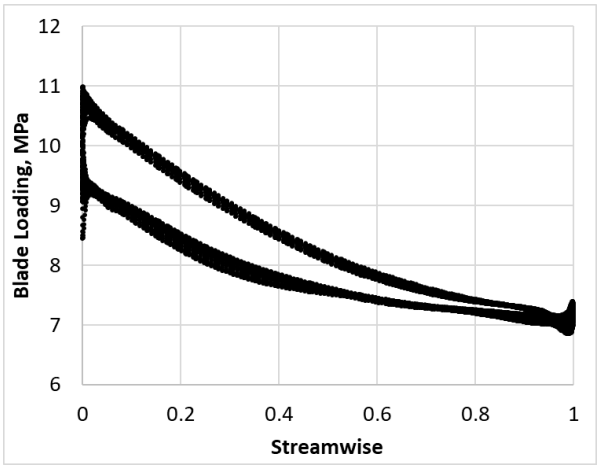

Figure 11: Blade loading at 0.5 span

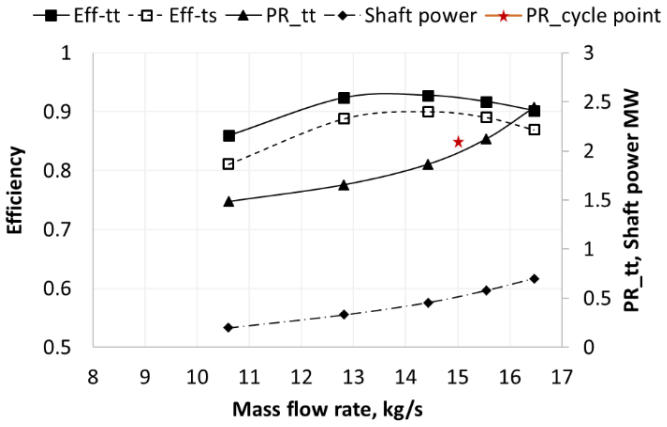

Figure 12: Performance map of the final design

THRUST PREDICTION

Usually, single-rotor expanders are an overhung design with bearing support provided to handle radial and axial loads (Figure 13). For this design, The rotor support includes oil film bearings to keep dynamic operation below the first critical speed and fluid film thrust bearings to large thrust loads during off-design conditions. As discussed previously, the focus is to develop a modular design that allows for the interchangeability of aerodynamic parts (volute, nozzle, and turbine stage) without modifying the generator, gearbox, and rotor support. The expander-generator rig is sized for 3 MW. However, performance validation under a laboratory environment required scaling down the aerodynamic section from 3 MW to 0.5 MW with an entirely different specific speed design. The scaling was done based on the flow loop's ability to handle the maximum flow rate. The temperature, inlet pressure, and pressure ratio were kept the same to size the turbine for lab-scale testing. While the simulated design meets the performance criterion, the unknowns surrounding the start-up conditions and thrust information necessitated quantifying the full numerical performance.

Thrust estimation relies upon analytical calculations by summing pressure and impulse forces over rotor surface areas. Those methods don't necessarily include factors such as blade loading and effects of seal geometries, and the deviation can be significant leading to either oversized or undersized bearings. CFD modeling is a more reliable method to quantify the thrust predictions and optimize the thrust balance. The majority of research [12][13][14] on thrust prediction methods focused on pumping devices, specifically multistage pumps due to high accumulated axial thrust and spatial restrictions to provide support in downhole applications. As for the radial expanders, the only reported work by Huo et al [15] focuses on numerical modeling to predict the effect of balance holes on thrust reduction. This section will focus on developing a numerical model to predict thrust information for the design and off-design conditions and different rotational speeds. One of the objectives of this study is to help make an informed choice regarding the start-up control scheme for the turbine loop using thrust information for different rotational speeds. The numerical model is shown in Figure 14. The model includes volute geometry with actual inlet size, nozzle vanes, shrouded rotor, front and back seals, and the diffuser. Low-specific speed turbine experience efficiency degradation due to leakage flow through front and back seals. Figure 15 shows the cross section of the mesh model with enlarged front and back seals. The front seal is designed to minimize the leakage flow, specifically, the low specific speed expanders struggle with efficiency degradation due to induced leakage flow as a function of the high-pressure ratio. The numerical methods and boundary conditions follow the previous section's model. Boundary conditions also include constant back pressure from the back seal side. Figure 16 shows the resulting velocity vectors across the front seal. The direct impingement of flow from the seal cavity generates circulation regions that oppose and creates a blockage effect. This is anticipated to

DOI: 10.17185/duepublico/77324

minimize the leakage flow. The front seal also includes swirl brakes to minimize the tangential velocity component for improved rotordynamic performance.

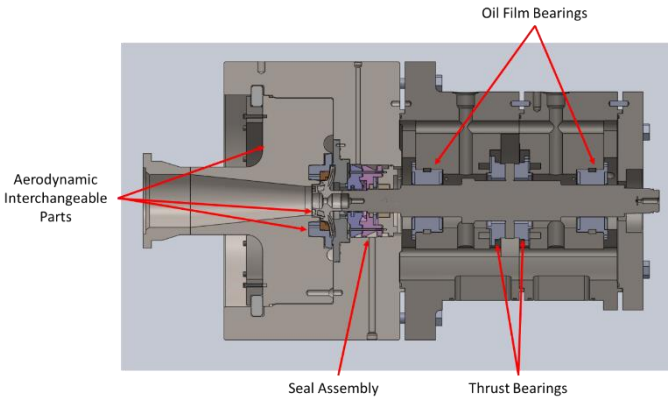

Figure 13: Designed expander section [10]

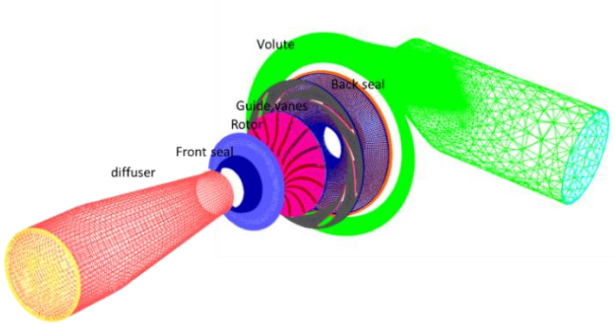

Figure 14: Numerical mesh model

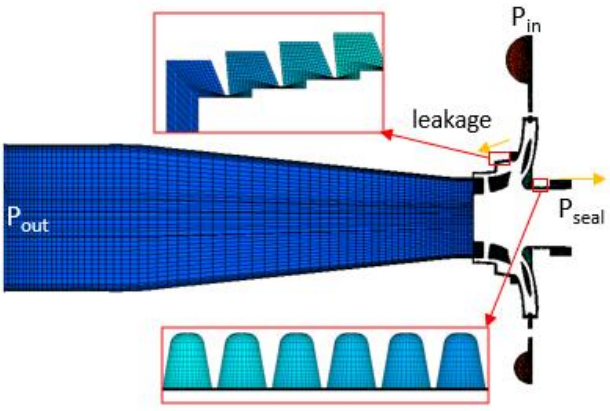

Figure 15: front back seal meshing

The front seal design creates an apparent blockage effect to minimize the leakage.

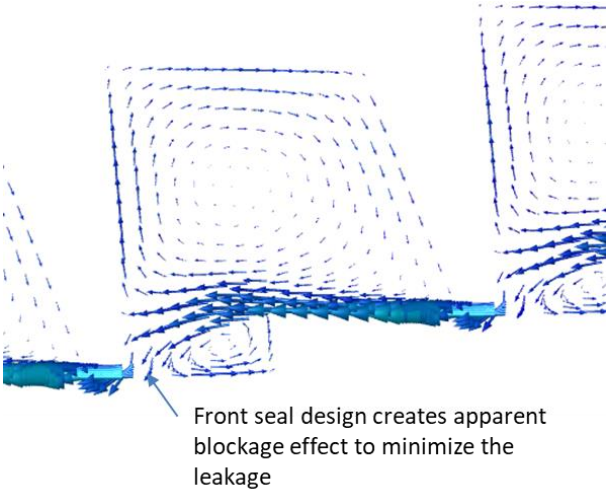

Figure 16: Velocity vectors in the front seal

Figure 17 shows the pressure distribution across rotor surfaces. Thrust is estimated by summing all the forces in the axial direction. Figure 18 shows the performance change due to the leakage flow through the front and back seals. The efficiency of the turbine degrades due to leakage flow through the seal by about ~9% compared to the model without the leakage flow included. Also, the additional flow passing through the leakage would shift the efficiency plot. One of the challenges the current rotor will face is difficulty in manufacturing the narrow aerodynamic path and achieving the required level of surface roughness. Increased surface roughness would induce additional friction losses resulting in efficiency degradation. Additional simulation by including surface roughness predicts performance reduction by ~13% compared to the base model.

Figure 19 shows axial thrust values as a function of different rotational speeds. Increased surface area at outlet side enable thrust direction from outlet to inlet for all the speeds. Increased rotational speed and mass flow rate (pressure ratio) results in reduced thrust force.

DOI: 10.17185/duepublico/77324

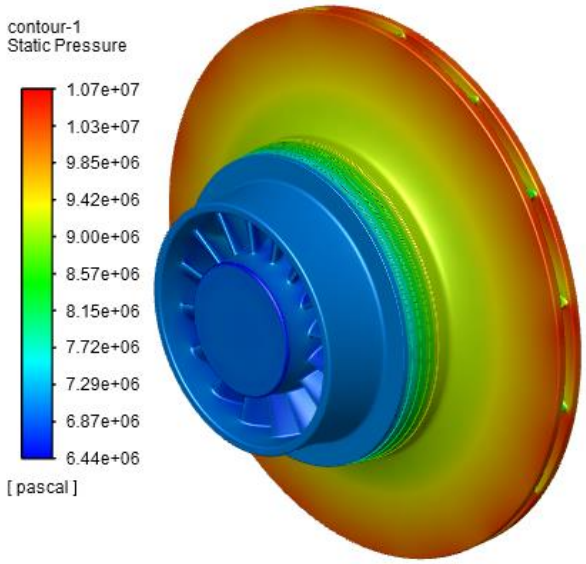

Figure 17: Pressure distribution

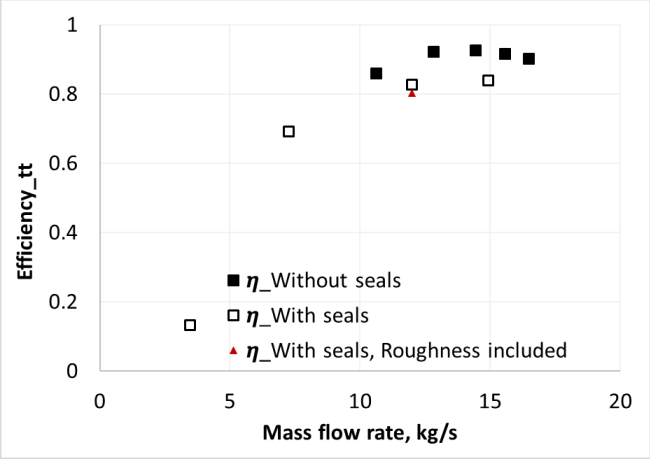

Figure 18: Total-to-total efficiency comparison

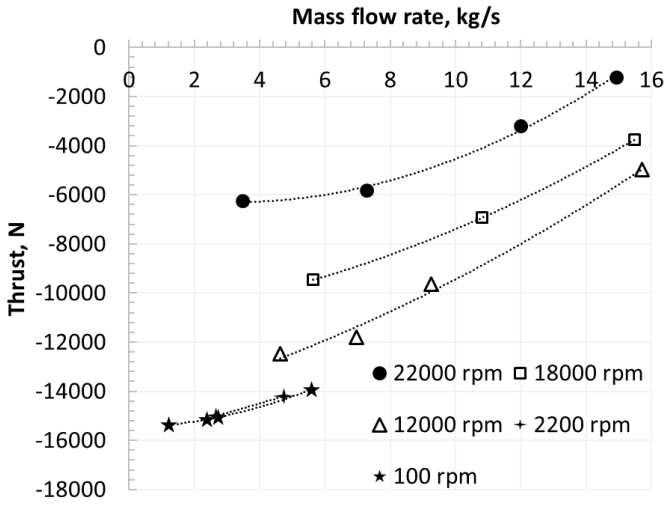

Figure 19: Thrust prediction at different rotational speeds

Initiating the turbine start-up can be challenging based on rotor configuration, weight, drag friction losses, and thrust load. The overall reactive load and torque outcomes from the performance data can be utilized to initiate the start-up and control mechanism.

CONCLUSION

The study presented a low-specific speed expander design approach using pseudo 1D and 3D modeling methods and numerical demonstration of the performance at design and off-design conditions. The outcomes from numerical investigations revealed the aerodynamic performance of nozzle guide vanes and the rotor highlighting areas for design improvement. Overall, the performance map of the proposed expander design meets the desired efficiency metric for the extended flow range. The full numerical modeling helped develop an improved understanding of the performance change due to the flow leakage through the front and back seals and thrust change for the wide range of operating speeds and flow rate conditions. The analysis outcomes reveal the flow losses could be significant due to the disc friction, incidence, and leakage flow path for low specific speed designs (9-13 % reduction in efficiency compared to the numerical model without seals included). Due to increased rotor surface at the outlet side, upthrust force increases with a reduction in rotational speeds and flow rate conditions. The analysis outcomes are incorporated in start-up and control schemes for the experimental investigation of the expander-generator unit in a laboratory environment.

ACKNOWLEDGEMENTS

This material is based upon work supported by Sage geosystems.

DOI: 10.17185/duepublico/77324

REFERENCES

[1] Bao J, Zhao L. A review of working fluid and expander selections for organic Rankine cycle. Renew Sustain Energy Rev. 2013;24:325–42.

[2] Garg P, Kumar P, Srinivasan K, Dutta K. Evaluation of isopentane, R-245fa and their mixtures as working fuids for organic Rankine cycles. Appl Therm Eng. 2013;51:292–300.

[3] Gong YL, Luo C, MA WB, WU ZJ. Thermodynamic analysis of geothermal power generation combined flash system with binary cycle, Proceedings World Geothermal Congress, 2010, Bali, Indonesia; 25–29 April; 2010.

[4] Flegkas, S., Klemencic, G., Haider, M., Werner, A., & Leibinger, H. (2016). "Comparison of Conventional and CO2Power Generation Cycles for Waste Heat Recovery", 1st European Seminar on Supercritical CO2 (sCO2) Power Systems, Wien, Austria.

[5] Wolf V., et al, 2022, "Investigation of sCO2 Cycle Layouts for the Recovery of Low Temperature Heat Source" The 7th International Supercritical CO2 Power Cycles Symposium, San Antonio.

[6] Hansper, J., et. al., 2019, "Assessment of Performance and Costs of Co2 based Geothermal Power Systems, 3rd European Conference on Supercritical CO2 (sCO2) Power Systems

[7] Katcher, K., et. al., 2021, "Estimated cost and Performance of a Novel sCO2 Natural Convection Cycle for Low-grade Waste Heat Recovery", The 4th European sCO2 Conference for Energy Systems

[8] https://www.sagegeosystems.com/sage-meta-unlocking-the-potential-of-geothermal-for-clean-compact-renewable-baseload-power/

[9] Nielson, Jordan, Kelsi Katcher, and Douglas Simkins. 2022. "Techno-Economic Analysis of a Geothermal SCO2 Thermosiphon Power Plant." The 7th International Supercritical CO2 Power Cycles Symposium.

[10] Nielson J., and Weiss N., 2022, Sage Geosystems Proprietary sCO2 Turbine Flow Loop Testing, GRC Transactions, Vol. 46, 2022

[11] Baines, N. C., 2005, "Radial Turbines: An Integrated Design Approach," Proceedings of the 6th European Turbomachinery Conference - Fluid Dynamics and Thermodynamics, Lille, France.

[12] Salvadori, S., Marini, A., and Martelli, F., 2012, "Methodology for the Residual Axial Thrust Evaluation in Multistage Centrifugal Pumps," Eng. Appl. Comput. Fluid Mech., 6(2), pp. 271–284.

[13] Zhou, L., Shi, W., Li, W., and Agarwal, R., 2013, "Numerical and Experimental Study of Axial Force and Hydraulic Performance in a Deep-Well Centrifugal Pump With Different Impeller Rear Shroud Radius," ASME J. Fluids Eng., 135(10), p. 10450

[14] Patil, Abhay & Kasprzyk, Marie & Adolfo, Delgado & Morrison, Gerald. (2019). Effect of Pump Leakage Flow PATH Wear On Axial Thrust in Downhole ESP Unit. Journal of Fluids Engineering. 142. 10.1115/1.4045571.

[15] Huo, C., Sun, J., Song, P., and Sun, S. (September 20, 2021). "Investigating the Influence of Impeller Axial Thrust Balance Holes on the Flow and Overall Performance of a Cryogenic Liquid Turbine Expander." ASME. J. Eng. Gas Turbines Power. October 2021; 143(10): 101014. https://doi.org/10.1115/1.4051501

DOI: 10.17185/duepublico/77324

DOI: 10.17185/duepublico/77324
URN: urn:nbn:de:hbz:465-20230427-145137-9